PHYSICAL REVIEW E VOLUME 60, NUMBER 5 NOVEMBER 1999

Critical angle of wet sandpiles

T. G. Mason, A. J. Levine,* D. Ertaş, and T. C. Halsey
Corporate Research, Exxon Research and Engineering Co., Route 22 East, Annandale, New Jersey 08801
(Received 23 November 1998; revised manuscript received 23 June 1999)

We measure the increase in the maximum stable angle of a sandpile, θ_c, with the volume fraction, ϕ, of a liquid added to cause cohesion between the grains. For two different liquids, $\tan\theta_c$ does not apparently scale with the air-liquid surface tension at low ϕ, whereas it does at higher ϕ. This suggests that the liquid forms menisci at asperities on the surfaces of the grains before filling cohesive menisci at intergrain contact points. In this cohesive limit, $\theta_c(\phi)$ agrees with a surface roughness theory. Electron and fluorescence microscopy of the dry and wet surfaces of the grains support this model. [S1063-651X(99)50411-X]

PACS number(s): 61.43.Gt, 62.20.Mk, 83.70.Fn

Cohesive forces between sand grains profoundly influence the macroscopic stability of sandpiles. A tiny volume of fluid that wets the sand can make the cohesion strong enough to greatly increase the pile's maximum angle of static stability, also known as the critical angle, θ_c [1]. Although this simple observation has been known for millennia, the relationships between the physical properties of the grains, the wetting fluid, and the macroscopic stability of the pile have remained obscure. Understanding these relationships can provide key insights into phenomena ranging from landslides to the stability of sand castles. Such relationships should clarify how small-scale surface properties dramatically influence large-scale mechanics [2]. In this, the problem of wet sand brings to mind the problem of friction in sandpiles, a problem to which it may even be related [3].

Piles of wet soil and wet sand are commonly observed to fail at depth. Classic Mohr-Coulomb analysis [1] applied to cohesive sandpiles reveals that the stability criterion governing θ_c depends on the cohesive stress due to the wetting fluid, s_A, relative to the gravitational stress at the failure depth, D [2],

$$k=\tan\theta_c\left(1+\frac{s_A}{\rho_B g D\cos\theta_c}\right)^{-1}, \qquad (1)$$

where k is the internal friction coefficient (equal to $\tan\theta_c$ for the dry pile), ρ_B is the mass density of the sandpile, and g is the gravitational acceleration. Equation (1) strictly predicts θ_c and not the ''angle of repose'' [1,4], which is typically smaller since it is measured after a dynamic event such as pouring or failure.

By considering how the wetting fluid occupies the microscopically rough surfaces between two spherical grains, it is possible to predict the intergrain cohesive force, f_A, as a function of added fluid volume per contact, V. Three distinct regimes have been proposed [2]. The *asperity regime* occurs for very low $V<V_1\approx l_R d^2$, where l_R is the roughness length scale corresponding to the asperity height and d is the average distance between asperities. Here, f_A is controlled by the surface roughness in the immediate neighborhood of the intergrain contact. Next, the *roughness regime* is encountered for $V_1<V<V_2\approx l_R^2 R$, where R is the grain's radius. Here, the Laplace pressure due to the fluid bridge between the grains is set by the asperity height (the grain's curvature does not play a role) and $f_A\propto V$. Finally, at large volumes $V>V_2$, the *spherical regime* is found where the grain's curvature is important and f_A does not depend on V. Using these results and Eq. (1), θ_c can be predicted as a function of the added fluid volume by assuming that the average V can be used at all contact points everywhere in the pile. This method, when applied to the roughness regime, qualitatively explains the linear rise in the angle of repose with added fluid volume observed in wet sandpiles using a draining crater method [5,6].

In this paper, we present measurements that explore the relationship between the pile's critical angle, the cohesive forces between the wet grains, and the surface roughness of the grains. We show that the increase in the critical angle with the ratio of added fluid volume to the volume of the grains, ϕ, is largely independent of the liquid-air interfacial tension, Γ, at very small ϕ, whereas it does scale linearly with Γ at larger ϕ. Optical fluorescence microscopy (OFM) of the distribution of fluid on the surface of the grains reveals inhomogeneities in intensity that may be attributed to liquid being trapped in menisci which form at asperities (i.e., protrusions) on the grain surfaces. This observation is consistent with scanning electron microscopy (SEM) images of the grains, which provide a direct image of their surface roughness. The sequestering of the liquid by asperities reduces the volume of liquid available to form cohesive menisci at the contact points between grains. This can account for the modest Γ-independent growth of the critical angle at low ϕ, and suggests that models that rely upon a large number of contact menisci having an average cohesive force may not be appropriate at extremely low ϕ. However, at larger ϕ, the linear scaling of $\theta_c(\phi)$ with Γ suggests that such models are appropriate, and we find that the behavior of $\theta_c(\phi)$ in this regime is entirely consistent with a scaling theory based on the surface roughness of the grains [2].

The sandpile is comprised of spherical glass grains; the measured mass density of the glass is $\rho=2.7\pm0.1$ g/cm^3. An SEM image of the bare, dry grains is shown in Fig. 1(a). The average sphere radius is $R=120\ \mu$m with a polydispersity of $\delta R/R=0.35$. A detailed view of the surface of a sphere,

*Present address: Department of Physics and Astronomy, University of Pennsylvania, 209 South 33rd St., Philadelphia, PA 19104.

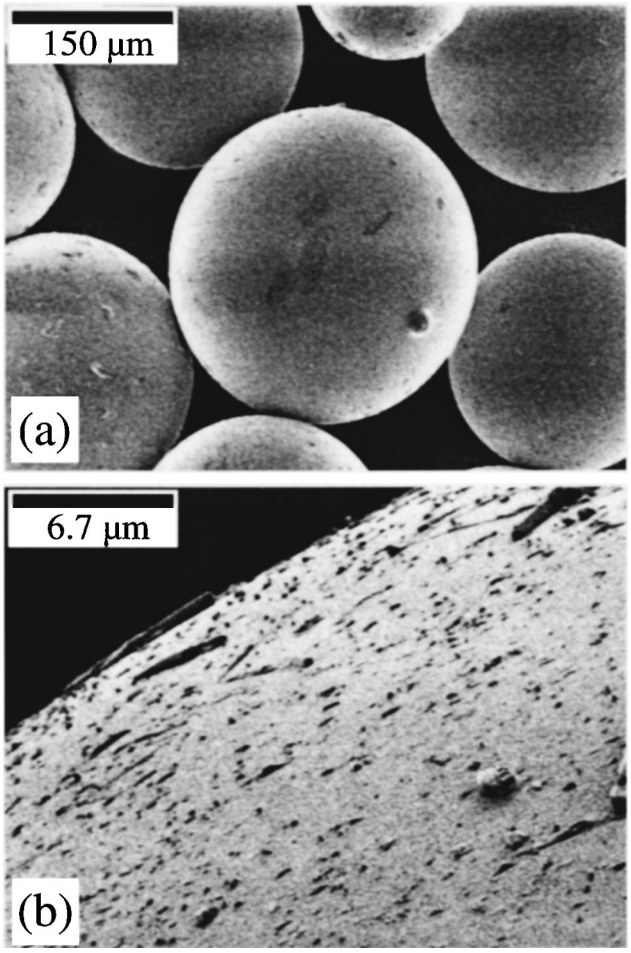

FIG. 1. SEM images of the dry surfaces of the glass spheres: (a) low magnification and (b) high magnification.

shown in Fig. 1(b), reveals a smooth glass surface with irregularly shaped microfragments of glass that are bonded to the sphere's surface. Due to the irregular nature of the shape and distribution of fragments on the surface, the roughness is difficult to characterize precisely. Large fragments of approximately 10 μm length and 1 μm height and width are found spaced at a center-to-center distance of about 20 μm, yet there are many smaller micron-sized bumps that are spaced several microns apart on average. Given these surface features, the length scale characterizing the roughness can vary significantly upon whether a number-averaged or volume-averaged size and spacing between the fragments is computed. For order of magnitude estimates, we use a roughness length scale, $l_R \approx 1\ \mu$m, to characterize the average height and width of the asperities, and we use an average distance between asperities of $d \approx 5\ \mu$m.

To measure the critical angle, θ_c, of the sandpile as a function of liquid volume fraction, we use the following procedure. A clear plastic box having a square bottom 6.5 cm wide and 5.5 cm high is filled to a depth of 2 cm with dry sand and a small amount of liquid is added. The sand grains have not been cleansed in any way. The top of the box is closed and sealed to limit possible evaporation and the sand is shaken at large amplitude for about 30 sec in order to distribute the liquid among the grains. This initial shaking is used to quickly distribute the droplet of wetting liquid from the top of the pile to all the grains. Without shaking, the

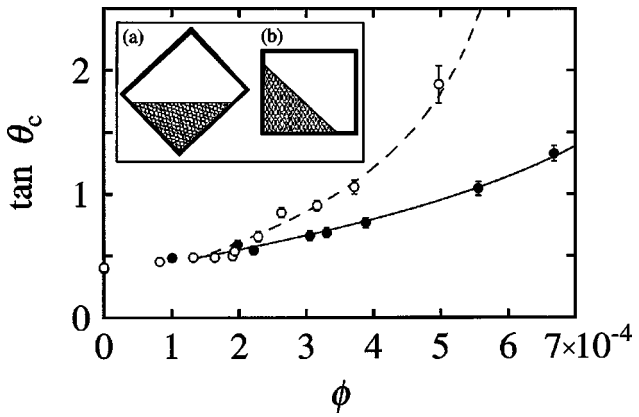

FIG. 2. Dependence of the tangent of the critical angle, tan θ_c, on the liquid to sphere volume fraction, ϕ, for C_{16} (closed circles) and DMSO (open circles). Fits using Eq. (3) above the critical filling fraction $\phi^* = 1.4 \times 10^{-4}$ are given by the solid (C_{16}) and dashed DMSO lines. Inset: Sand in the box is shaken normal to the page to form a pile resembling a wedge (a). The box is slowly rotated about its edge until it rests flat on a horizontal surface (b).

transport of the wetting liquid from this droplet to the surfaces of the grains in the bulk of the pile is too slow to make the measurements of θ_c practical. This 30 sec duration of the initial shaking is adequate to distribute the liquid evenly within the pile because doubling this shaking time does not lead to a difference in the measured θ_c. Because the surface area associated with the walls of the container is much less than the surface area on the grains, any loss of the wetting fluid to the container walls can be neglected. Since the interior corners and edges of the box are rounded with a radius of curvature much larger than the grain radius, the wetting fluid cannot be trapped there, so any loss of the wetting fluid to corners or edges can also be neglected. The box is then tilted on its edge and the wet grains are shaken back and forth along the direction of the edge until they form an even surface normal to the direction of gravity. After shaking to distribute the grains in the wedge, we measure their volume fraction of packing, v, to be $v = 0.61 \pm 0.02$, indicating the spheres are loosely rather than closely packed. This value reflects a spatial average over the entire pile and does not account for possible inhomogeneities in v that could result from preparing the wedge by shaking. The edge of the box is then placed on a horizontal surface and the box is slowly rotated about its edge until it rests flat on the table, as shown in Fig. 2 [insets (a) and (b)]. During this slow rotation, the grains are not fluidized, but static. If the sandpile fails catastrophically at depth during the rotation, no measurement is made. If it does not, then the height and base of the pile are measured. For a given ϕ, the three trials yielding the largest θ_c out of a total of five or six trials are averaged to obtain θ_c. This procedure provides an accurate way of measuring the maximum static critical angle and not the more commonly encountered angle of repose associated with flowing sand.

In order to examine the role of the interfacial tension in setting the critical angle, we have measured $\theta_c(\phi)$ for two different liquids with significantly different Γ. We have intentionally avoided water because of potential problems with evaporation and humidity control [3]. Pendant drop measure-

ments of hexadecane (C_{16}) yield $\Gamma_{C16}=28.1$ dyn/cm and of dimethyl sulfoxide (DMSO) yield $\Gamma_{DMSO}=46.6$ dyn/cm. We have attempted to measure how both of these liquids wet glass using an AST Video Contact Angle device, and we find that the wetting is so strong that the contact angles are much less than the instrument's 5° resolution limit. In Fig. 2, the closed and open circles represent measurements of $\tan\theta_c$ made using C_{16} and DMSO, respectively. There is a very weak rise from $\tan\theta_c\approx 0.4$ at $\phi=0$ to $\tan\theta_c\approx 0.5$ at $\phi\approx 1.5\times 10^{-4}$. Beyond this ϕ, the rise in $\tan\theta_c(\phi)$ becomes more pronounced, and the increase for DMSO is larger than that for C_{16}. The rapid increase in $\tan\theta_c$ and the larger error bars at large ϕ reflect the fact that $\tan\theta_c$ is approaching a divergence in which the cohesion can support a vertical wall.

To directly image the distribution of fluid on and between the glass spheres after shaking, we employ fluorescence confocal microscopy. A Bodipy dye in DMSO exhibits good solubility and has excitation and emission wavelengths that are matched with the illuminating laser and bandpass detection filter, providing measurable fluorescence at very small ϕ. Any residual dye particles are removed by filtration. Due to the large size of the spheres compared to the working distance of the objective, we are able to scan vertically only up to the midplane of the first layer of spheres resting on the slide's surface. The midplane view permits us to examine the fluid near the contact points between spheres.

After adding the dyed DMSO at $\phi=2.1\times 10^{-4}$ to a dry sandpile, shaking, and removing a small quantity of the wet sand, we measure the fluorescent intensity of the dyed fluid on the surface of the spheres, as shown in Fig. 3(a). The bright circles indicate that the wetting fluid has spread over the surfaces of all the spheres, confirming that the shaking procedure does distribute the fluid evenly within the pile. However, the fluorescent intensity does vary azimuthally around each of the circles, indicating that the distribution of fluid over the surface of a single sphere is nonuniform. This suggests that capillary forces can pin the fluid to the surface irregularities, so that the distribution of fluid on the surface cannot be described simply by a single wetting film thickness, as in [2]. At apparent points of contact between neighboring spheres, the resolution is insufficient to provide much information about the structure of the fluid there, although it is clear that a large quantity of the fluid on the surface has not migrated to the contact points. At a much larger volume fraction of fluid, $\phi\approx 10^{-2}$, we find that it is possible to image fluid forming hour-glass shaped menisci at the contact points between spheres, as indicated by the halolike intensities shown in Fig. 3(b).

Both the macroscopic measurements of the critical angle and the microscopic observations of the roughness and inhomogeneous wetting of the grain surfaces can be reconciled by the following physical model. At extremely low ϕ, the wetting liquid is trapped in tiny menisci which form between the edges of jagged asperities and the flat surface of the grains. If the grains have a large number of small asperities, the wetting fluid becomes trapped in these menisci and does not migrate to the cohesive contact menisci between grains where they touch, because such menisci would have larger radii of curvature. The nonparticipating menisci become filled at a threshold volume fraction, ϕ^*. In the *fluid-depleted regime*, $\phi<\phi^*$, the cohesive forces between grains

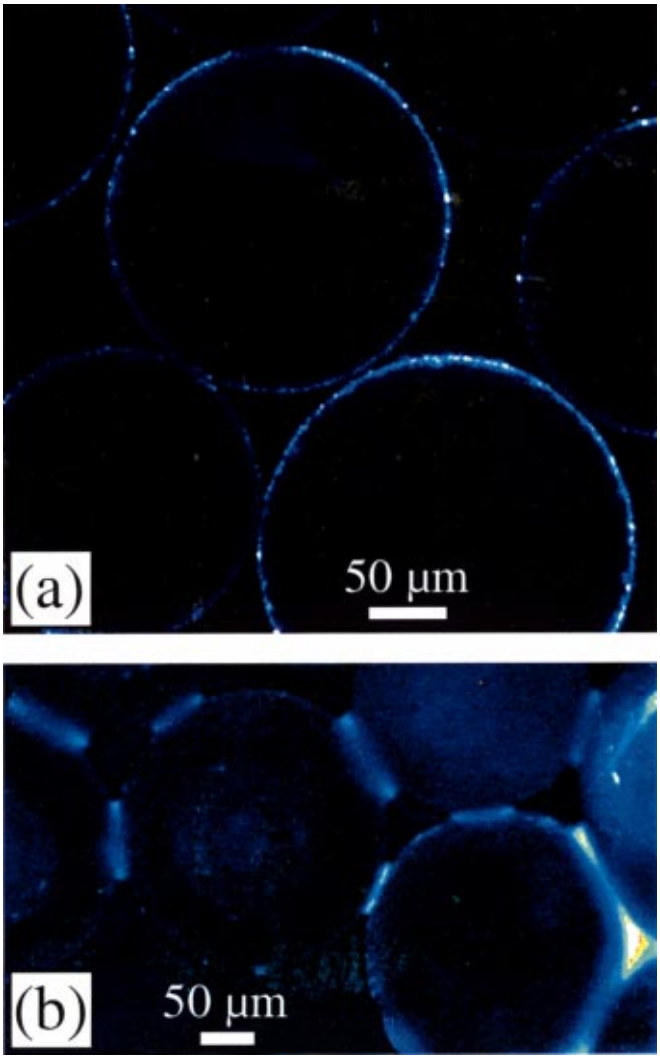

FIG. 3. (Color.) Fluorescence microscopy images of DMSO on the surface of the grains: (a) $\phi=2.1\times 10^{-4}$ and (b) $\phi\approx 10^{-2}$.

are small because only a small fluid fraction occupies the intergrain contacts. However, in the *fluid-excess regime* for $\phi>\phi^*$, the extra fluid (in excess of ϕ^*) fills the contact menisci and provides a homogeneous cohesive force between grains. For an average grain coordination number of z, the fluid volume per contact is $V=8\pi R^3(\phi-\phi^*)/(3z)$. In the roughness regime, f_A is the Laplace pressure of the contact meniscus, Γ/l_R, times the wetted contact area, V/l_R, i.e., $f_A\approx\Gamma V/l_R^2$. For a grain packing fraction of $\nu=\rho_B/\rho$, the average cohesive stress is $s_A=z\nu f_A/(4\pi R^2)$. The dimensionless cohesive stress, $\alpha\equiv s_A/(\rho_B g D)$, is

$$\alpha=2\Gamma R(\phi-\phi^*)/(3l_R^2\rho g D). \tag{2}$$

Thus, α scales linearly with Γ and excess volume fraction and is independent of z and ν.

The beginning of the roughness regime can be identified from Fig. 2. The increase in $\tan\theta_c(\phi)$ does not depend on Γ below a threshold volume fraction of $\phi^*\approx 10^{-4}$. To determine if this is physically consistent with the model, we estimate the volume fraction required to fill the nonparticipating menisci: $\phi^*\approx l_R^3/(d^2R)$. This represents the fluid volume in the average asperity times the number of asperities on the

surface of a grain, divided by the total grain volume. Using $l_R \approx 1\ \mu$m, $d \approx 5\ \mu$m and $R = 120\ \mu$m we estimate $\phi^* \approx 3 \times 10^{-4}$; the fluid in the wetting film can be neglected. Given the crudeness of this estimate, this value is quite close to the observed $\phi^* \approx 1.5 \times 10^{-4}$. Using this ϕ^* and V_2, we estimate that the roughness regime corresponds to $\phi^* \lesssim \phi \lesssim \phi^* + 3zl_R^2/(8R^2)$, or $1.5 \times 10^{-4} \lesssim \phi \lesssim 3 \times 10^{-4}$ (for $z \approx 6$ [7]). Moreover, we believe that the value of ϕ^* implies that the fluid sequestration in nonparticipating menisci essentially camouflages the asperity regime, making it unobservable in our experiments.

Above ϕ^*, $\tan\theta_c(\phi)$ does depend on Γ, and its slope is distinguishably larger for DMSO than for C_{16}. We solve Eq. (1) explicitly for $\tan\theta_c$ and find

$$\tan\theta_c = k\left(\frac{1+\alpha\sqrt{1+k^2-\alpha^2k^2}}{1-\alpha^2k^2}\right), \tag{3}$$

where $k = \tan\theta_c(\phi = \phi^*)$ is redefined to be the effective internal friction coefficient when contact menisci begin to form. This expression captures both the linear rise in $\tan\theta_c$ just above ϕ^* where α is small as well as the nonlinear divergence where $\alpha = 1/k$. Using Eq. (3), we fit the measured $\tan\theta_c(\phi)$ above the empirically observed crossover, choosing $\phi^* = 1.4 \times 10^{-4}$ and $k = 0.49$. We set $\alpha = C(\phi - \phi^*)$, where the only fitting parameter is $C \equiv 2\Gamma R/(3\rho g D l_R^2)$. The results of the fits are shown by the solid line ($C_{C16} = 1920$) and the dashed line ($C_{DMSO} = 3620$) in Fig. 2. The agreement between the fits and the data are good; moreover, the ratio $C_{DMSO}/C_{C16} = 1.88$ is only about ten percent higher than the expected ratio of $\Gamma_{DMSO}/\Gamma_{C16} = 1.66$ based on simple scaling with surface tension. Using the measured Γ_{C16} and taking $D \approx 2$ cm, we would have predicted $C_{C16} \approx 4250$, a little more than two times the fitted value. Given the uncertainty in SEM value for l_R and the lack of precise numerical prefactors of order unity in the expression for C, the overall magnitude of the data are in good agreement with the theory. Other choices of ϕ^* and k consistent with the observed crossover do not strongly influence the quality of the fits or the values of C.

Our data indicate that piles can develop a diverging $\tan\theta_c$ while the cohesive contact forces between grains remain in the roughness regime. An investigation of the predicted asperity regime is precluded by the formation of nonparticipating menisci, and the saturation of θ_c in the spherical regime is not seen because $\tan\theta_c$ has diverged at lower ϕ. In fact, smaller spheres which preserve $R/l_R \approx 100$ should exhibit a diverging $\tan\theta_c$ at much lower liquid volumes: ϕ^* will go down and C will increase. This is consistent with the commonly observed sensitivity to humidity of the critical angle in very fine powders. In principle, measurements of the macroscopic $\theta_c(\phi)$ could be used to estimate l_R if the average grain size, pile depth, grain density, and surface tension are known. For wet sandpiles comprised of faceted or jagged grains, it would be intriguing to understand how different grain shapes can affect $\theta_c(\phi)$ both experimentally and theoretically.

In conclusion, we have studied how the critical angle of a well-characterized sandpile depends on ϕ and Γ. We have identified a threshold volume fraction, ϕ^*, above which $\tan\theta_c$ is observed to depend on Γ. For $\phi < \phi^*$, the liquid is driven by the Laplace pressure into nonparticipating menisci. The modest rise in $\theta_c(\phi)$ for $\phi < \phi^*$ is presumably due to the formation of relatively weak contact menisci. Although the precision of the data in this regime is limited, the apparent absence of scaling of $\tan\theta_c(\phi)$ with Γ there may indicate that an inhomogeneous distribution of intergrain cohesive contact forces exists within the pile. By contrast, for $\phi > \phi^*$, the nonparticipating menisci are filled, the excess liquid accumulates in the contact menisci, and the data for $\tan\theta_c(\phi)$ are consistent with cohesive forces that are uniform in distribution and strength. Although we have not measured the distribution of microscopic cohesive forces within the pile, the data for $\theta_c(\phi)$ in the Γ-scaling fluid-excess regime are consistent with the predicted Mohr-Coulomb failure criterion applied to the roughness regime [2].

We thank J. McHenry and R. Johnston for help with the microscopy and J. Hutter for help with the interfacial tension measurements.

[1] R. M. Nedderman, *Statics and Kinematics of Granular Materials* (Cambridge University Press, Cambridge, England, 1992).

[2] T. C. Halsey and A. J. Levine, Phys. Rev. Lett. **80**, 3141 (1998).

[3] L. Bocquet, E. Charlaix, S. Ciliberto, and J. Crassous, Nature (London) **396**, 735 (1998).

[4] H. M. Jaeger, C.-H. Liu, and S. R. Nagel, Phys. Rev. Lett. **62**, 40 (1989).

[5] D. J. Hornbaker, R. Albert, I. Albert, A.-L. Barabási, and P. Schiffer, Nature (London) **387**, 765 (1997)

[6] R. Albert, I. Albert, D. Hornbaker, P. Schiffer, and A.-L. Barabási, Phys. Rev. E **56**, R6271 (1997).

[7] A. Mehta and G. C. Barker, Phys. Rev. Lett. **67**, 394 (1991).